

# Spatially resolved mid-infrared observations of the circumstellar environment of the born-again object FG Sge <sup>★</sup>

K. Ohnaka<sup>1</sup> and B. A. Jara Bravo<sup>1</sup>

Instituto de Astrofísica, Universidad Andrés Bello, Fernández Concha 700, Las Condes, Santiago, Chile  
e-mail: k1.ohnaka@gmail.com

Received / Accepted

## ABSTRACT

**Context.** FG Sge has evolved from the hot central star of the young planetary nebula Hen 1-5 to a G–K supergiant in the last 100 years. It is one of the three born-again objects that has been identified as of yet, and they are considered to have undergone a thermal pulse in the post-asymptotic giant branch evolution.

**Aims.** We present mid-infrared spectro-interferometric observations of FG Sge and probe its dusty environment.

**Methods.** FG Sge was observed with MIDI at the Very Large Telescope Interferometer at baselines of 43 and 46 m between 8 and 13  $\mu\text{m}$ .

**Results.** The circumstellar dust environment of FG Sge was spatially resolved, and the Gaussian fit to the observed visibilities results in a full width at half maximum of  $\sim 10.5$  mas. The observed mid-infrared visibilities and the spectral energy distribution can be fairly reproduced by optically thick ( $\tau_V \approx 8$ ) spherical dust shell models consisting of amorphous carbon with an inner radius  $r_{\text{in}}$  of  $\sim 30 R_\star$  (corresponding to a dust temperature of  $1100 \pm 100$  K). The dust shell is characterized with a steep density profile proportional to  $r^{-3.5 \pm 0.5}$  from the inner radius  $r_{\text{in}}$  to  $(5 - 10) \times r_{\text{in}}$ , beyond which it changes to  $r^{-2}$ . The dust mass is estimated to be  $\sim 7 \times 10^{-7} M_\odot$ , which translates into an average total mass-loss rate of  $\sim 9 \times 10^{-6} M_\odot \text{ yr}^{-1}$  as of 2008 with a gas-to-dust ratio of 200 being adopted. In addition, the 8–13  $\mu\text{m}$  spectrum obtained with MIDI with a field of view of 200 mas does not show a signature of the polycyclic aromatic hydrocarbon (PAH) emission, which is in marked contrast to the spectra taken with the Spitzer Space Telescope six and 20 months before the MIDI observations with wide slit widths of  $3''.6\text{--}10''$ . This implies that the PAH emission originates from an extended region of the optically thick dust envelope.

**Conclusions.** The dust envelope of FG Sge is much more compact than that of the other born-again stars' Sakurai's object and V605 Aql, which might reflect the difference in the evolutionary status. The PAH emission from the extended region of the optically thick dust envelope likely originates from the material ejected before the central star became H-deficient, and it may be excited by the UV radiation from the central star escaping through gaps among dust clumps and/or the bipolar cavity of a disk-like structure.

**Key words.** infrared: stars – techniques: interferometric – stars: circumstellar matter – stars: carbon – stars: AGB and post-AGB – stars: individual: FG Sge

## 1. Introduction

FG Sge is the central star of the young planetary nebula Hen 1-5 and a very rare object whose evolution can be observed in a lifetime of a human being. In the last 100 years, it has rapidly evolved redward on the Hertzsprung–Russell (H–R) diagram, from the hot central star of the planetary nebula (effective temperature  $T_{\text{eff}} \approx 40\,000$  K) to a G supergiant ( $T_{\text{eff}} \approx 5500$  K, Jeffery & Schönberner 2006). The rapid evolution of FG Sge is considered to be caused by a late thermal pulse (LTP) that occurs after the asymptotic giant branch (AGB), when the star is evolving blueward and almost horizontally on the H–R diagram. The nuclear energy produced by the thermal pulse results in the expansion of the thin outer layers on a timescale of 50 to a few 100 years, and the star evolves rapidly redward on the H–R diagram, turning into a so-called born-again object (e.g., Langer et al. 1974; Iben 1976; Blöcker 2001). When the temperature of the expanding outer layers becomes low enough for convection to penetrate to deep layers, the nuclear-processed material,

such as C, He, and *s*-process elements, is dredged up to the surface. Since the mass of the H-rich outer layers is already small, this dredge-up process makes the atmosphere H-deficient and C-rich. After the surface temperature reaches its minimum of several 1000 K, the star evolves again blueward on a timescale of  $10^3\text{--}10^4$  years finally to a white dwarf.

The final flash episode is so brief that objects such as FG Sge are very rare. Only three objects are known to date: FG Sge, Sakurai's object (V4334 Sgr), and V605 Aql. The evolution of FG Sge back to the AGB over  $\sim 100$  years is consistent with the LTP scenario, while the return of Sakurai's object and V605 Aql to the AGB is even more rapid on the order of several years. They are considered to have experienced the so-called very late thermal pulse (VLTP) – a thermal pulse that occurs when the star is evolving downward to a white dwarf on the H–R diagram (Clayton et al. 2006). In addition, Reindl et al. (2017) recently found that SAO244567, the central star of the Stingray nebula, has been rapidly returning to the AGB since 2002, and they conclude that it has undergone an LTP. The final flash episode is considered to be a fairly common phenomenon, which occurs in 10–20% of stars evolving off the AGB (Blöcker 2001; Herwig 2005). Therefore, studies of final flash objects provide a unique

Send offprint requests to: K. Ohnaka

<sup>★</sup> Based on observations made with the Very Large Telescope Interferometer of the European Southern Observatory. Program ID: 081.D-0244

opportunity to obtain insight into the evolution of post-AGB stars.

Although FG Sge is discussed as an LTP object in the literature (e.g., Schönberner 2008), the evolution of its chemical composition is not yet fully understood. The detailed spectroscopic analysis of Jeffery & Schönberner (2006) shows that the atmosphere of FG Sge became H-deficient some time between 1960 and 1995, and the detection of C<sub>2</sub> (Iijima & Strafella 1993; Kipper & Kipper 1993) reveals that the atmosphere is C-rich. However, this photospheric chemical composition of FG Sge and its evolution on the H-R diagram cannot be consistently explained by the present stellar evolutionary theory as discussed by Jeffery & Schönberner (2006). The calculations of born-again giants (Blöcker 2001) predict that the atmosphere becomes H-deficient only after the star begins to evolve blueward again (i.e., when the temperature is increasing again). However, FG Sge became H-deficient between 1960 and 1995, when the surface temperature was still decreasing. In the case of a VLTP, hydrogen in the outer layers becomes significantly depleted due to the hydrogen burning during the helium flash (Herwig et al. 1999). This means that the star is already H-deficient when it begins to evolve redward. However, FG Sge was H-normal in 1960 when it was evolving redward. The alternative double-loop scenarios proposed by Lawlor & MacDonald (2003) and Miller Bertolami et al. (2006), in which FG Sge, Sakurai’s object, and V605 Aql can be considered to represent different evolutionary stages of the same evolutionary path, cannot entirely explain the observed chemical composition of FG Sge either, as Jeffery & Schönberner (2006) have discussed.

Another remarkable change occurred in FG Sge in 1992, when its visual brightness decreased suddenly by  $\Delta V \approx 5$  magnitude and recovered gradually over the course of  $\sim 1$  year. Since then, FG Sge has shown sudden, unpredictable deep declines at an interval of 1–2 years; although, such events have become so frequent that the central star has been seldom visible since 2008 (Arhipova et al. 2022). At the same time, it started to show a noticeable infrared excess characterized by carbonaceous dust with  $\sim 1000$  K (Gehrz et al. 2005). The light curve of FG Sge is similar to those of R CrB stars – a class of F–G supergiants in which optically thick dust clouds are ejected in random directions – and an occasional, deep decline is observed when a cloud happens to form in the line of sight (Clayton 1996). While some authors propose that FG Sge is undergoing such a random dust cloud formation (Gonzalez et al. 1998), Gehrz et al. (2005) have argued for a continuous outflow with abrupt, episodic changes of the mass-loss rate. In either case, however, it is unknown where and how dust can form around FG Sge, whose present temperature (4500–5500 K) is deemed to be too high for dust to condense.

To obtain a clearer picture of the dusty environment of FG Sge, high spatial resolution mid-infrared observations are effective. In this paper, we present the first spatially resolved mid-infrared (8–13  $\mu\text{m}$ ) observations of FG Sge and radiative transfer modeling of its circumstellar envelope.

## 2. Observations

FG Sge was observed with the MIDI instrument (Leinert et al. 2003) at ESO’s Very Large Telescope Interferometer (VLTI) on 2008 June 22 (MJD54639) using the unit telescope (UT) configuration UT2–UT3 with projected baseline lengths of 43–46 m (Program ID: 081-D0224, P.I.: K. Ohnaka). A prism with a spectral resolution of  $\lambda/\Delta\lambda \approx 30$  (at 10  $\mu\text{m}$ ) was used to obtain spectrally dispersed fringes in the *N* band between 8 and 13  $\mu\text{m}$ .

**Table 1.** MIDI observations of FG Sge and the calibrator: time of observation (coordinated universal time=UTC), projected baseline length  $B_p$ , position angle of the projected baseline on the sky (P.A.), seeing in the visible, and the airmass at the times of the observations of FG Sge and the calibrator.

#	Object	$t_{\text{obs}}$ (UTC)	$B_p$ (m)	P.A. ( $^\circ$ )	Seeing ( $''$ )	Airmass
2008 June 22 (MJD2454639)						
CAL1	HD168723	07:27:42	46.0	46	1.0	1.35
SCI1	FG Sge	07:46:02	43.0	50	1.0	1.47
CAL2	HD168723	08:36:15	43.3	43	1.0	1.84
SCI2	FG Sge	08:57:21	45.9	47	1.0	1.74
SCI3	FG Sge	09:06:47	46.1	46	1.1	1.82

The data were taken in SCI-PHOT mode, in which photometric data of each telescope are recorded simultaneously with interferometric data. A detailed description of the observing procedure is given in Przygodda et al. (2003), Leinert et al. (2004), and Chesneau et al. (2005). Table 1 summarizes the observations’ FG Sge and the calibrator.

We used the MIA+EWS package ver.2.0<sup>1</sup> to reduce the MIDI data (Leinert et al. 2004; Jaffe 2004). We adopted a uniform-disk diameter of 3.1 mas for the calibrator HD168723 (Bourges et al. 2017). It should be noted that there are significant differences in airmass among the data sets. To avoid systematic errors, we calibrated the data sets of FG Sge with those of the calibrator taken at a similar airmass: the data set SCI1 was calibrated with CAL1, while the data sets SCI2 and SCI3 were calibrated with CAL2.

We assessed the data quality and derived the calibrated visibilities as described by Ohnaka et al. (2008). Because it is difficult to estimate the errors in the calibrated visibilities properly from two calibrator data sets taken at very different airmasses, we assumed a total relative error of 10% as adopted by Zhao-Geisler et al. (2011) for SCI-PHOT mode data. Because the projected baseline length and position angle of SCI2 and SCI3 are very close, we averaged the calibrated visibilities of these two data sets. The visibilities obtained with MIA and EWS agree well, and we only provide the results derived with EWS in the discussion below.

The absolutely calibrated *N*-band spectra of FG Sge were obtained from the same three SCI–CAL pairs taken at similar airmasses (SCI1–CAL1, SCI2–CAL2, and SCI3–CAL2), using the method described in Ohnaka et al. (2007). The average and the standard deviation of the three spectra were taken as the final spectrum and its error, respectively.

We also obtained the 19.5  $\mu\text{m}$  flux of FG Sge with the mid-infrared imager and spectrograph VLT/VISIR (Lagage et al. 2004). The VISIR observations of FG Sge and a photometric standard star, HD173780, were carried out on 2008 May 30, about three weeks before the MIDI observations, with the Q3 filter (central wavelength = 19.5  $\mu\text{m}$ , filter full width at half maximum = 0.4  $\mu\text{m}$ ) and a pixel scale of 0 $''$ .075. The data with chopping and nodding were first reduced using the VISIR pipeline ver.3.0.0 to obtain the images with the sky background almost subtracted. From these images, we further subtracted the residual sky background measured in an annular region with an inner and outer radius of 1 $''$ .5 and 2 $''$ .25, respectively. The flux was

<sup>1</sup> Available at <http://www.strw.leidenuniv.nl/~nevec/MIDI>

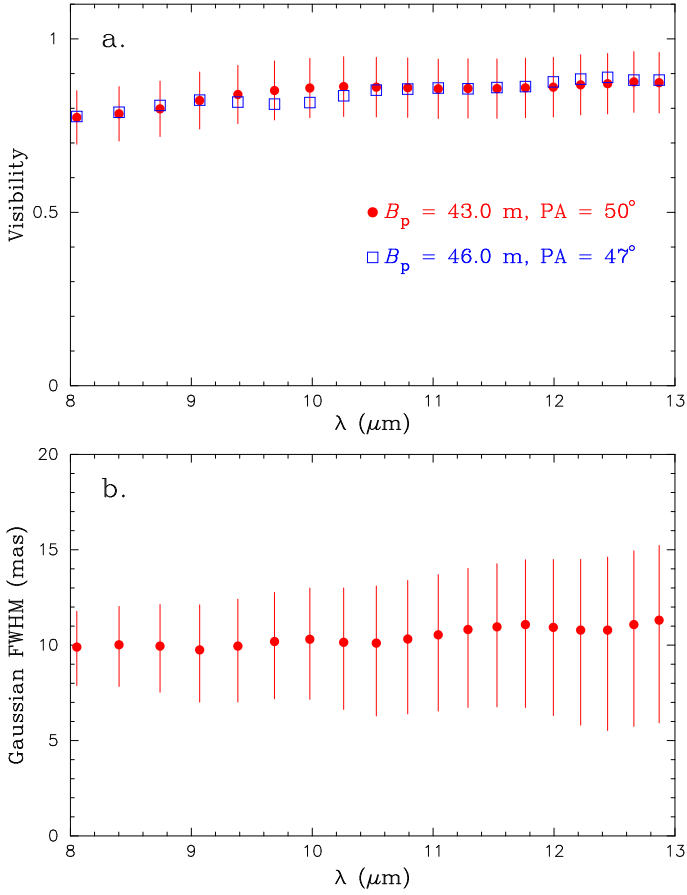


**Fig. 1.** VLT/MIDI observations of FG Sge. **a:** Observed visibilities of the data set SCI1 (red dots) and the average of SCI2 and SCI3 (blue dots). The error bars are only shown for the data set SCI1 for visual clarity. **b:** FWHM obtained by a Gaussian fit to the observed visibilities.

obtained within an aperture radius of  $1''.5$  both for FG Sge and HD173780, and the data of FG Sge were flux-calibrated with a Q3-band flux of  $1.7276$  Jy for HD173780<sup>2</sup>. The error in the calibrated flux of FG Sge was estimated by the quadratic sum of the photon noise of the source and that of the background. The observed  $19.5$   $\mu\text{m}$  flux of FG Sge is  $6.2 \pm 0.49$  Jy.

### 3. Results

Figure 1a shows the measured  $N$ -band visibilities, which slightly increase from  $0.8$  at  $8$   $\mu\text{m}$  to  $0.9$  at  $13$   $\mu\text{m}$ . Figure 1b shows the full width at half maximum (FWHM) obtained by the Gaussian fitting, which suggests that the observed visibilities correspond to an approximately constant FWHM of  $\sim 10.5$  mas. The observed visibilities suggest that the dust envelope of FG Sge is compact compared to the other born-again objects' Sakurai's object and V605 Aql. Chesneau et al. (2009) showed that the MIDI visibilities of Sakurai's object obtained at baseline lengths of  $42$ – $46$  m – the same as in our observations of FG Sge – range from  $0.05$  to  $0.2$ , which is much lower (thus much more extended) than the  $0.8$ – $0.9$  obtained for FG Sge; although, the distance to two objects is comparable (FG Sge:  $3.0$  kpc, Sakurai's object:  $3.8$  kpc, Evans et al. 2020). Clayton et al. (2013) report that

<sup>2</sup> [https://www.eso.org/sci/facilities/paranal/instruments/visir/tools/zerop\\_cohen\\_Jy.txt](https://www.eso.org/sci/facilities/paranal/instruments/visir/tools/zerop_cohen_Jy.txt)

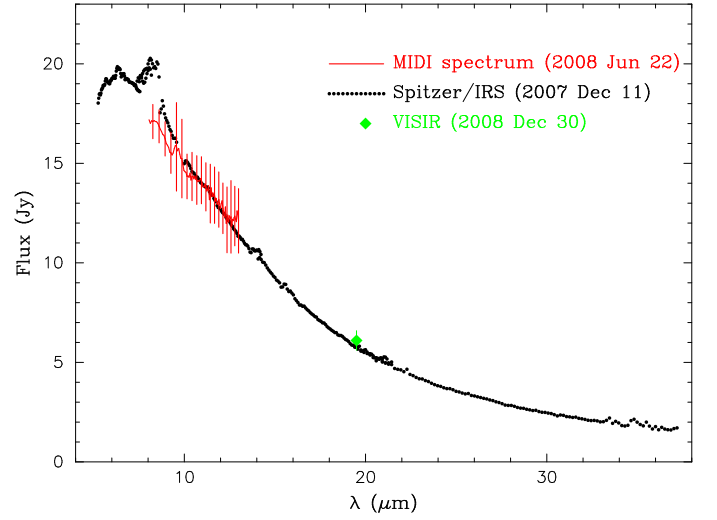


**Fig. 2.** Observed mid-infrared spectrum of FG Sge. The solid red line with the error bars shows the MIDI spectrum. Black dots correspond to the Spitzer/IRS spectrum. The green diamond is the VISIR Q3-band ( $19.5$   $\mu\text{m}$ ) flux.

V605 Aql was so large that it was resolved out in the MIDI observations with UT2 and UT3 (the same as used for FG Sge) in spite of its distance of  $4.6$  kpc. This is primarily because the effective temperature of FG Sge ( $4500$ – $5500$  K, see Sect. 4) is noticeably lower than those of Sakurai's object ( $12000$  K, van Hoof et al. 2007) and V605 Aql ( $95000$  K, Clayton et al. 2006). In addition, the luminosity of these latter objects ( $\sim 10^4 L_{\odot}$ , Schönberner 2008; Chesneau et al. 2009) is higher than that of FG Sge ( $4850^{+4600}_{-2690} L_{\odot}$ , Sect. 4), which can also make them appear larger than FG Sge.

Figure 2 shows the MIDI spectrum (red solid line with the error bars) and the  $19.5$   $\mu\text{m}$  flux measured with VISIR (green filled diamond). To complement the MIDI  $N$ -band spectrum and the VISIR  $Q$ -band photometric data, we downloaded the mid-infrared spectrum taken with the InfraRed Spectrograph<sup>3</sup> (IRS, Houck et al. 2004) onboard the Spitzer Space Telescope (Werner et al. 2004)<sup>4</sup>. The data were taken on 2007 December 11 (MJD 54446) in the short and long low mode with spectral resolutions of  $64$ – $128$ , covering from  $5$  to  $40$   $\mu\text{m}$  (Program ID: 40061, P.I.: A. Evans).

The  $19.5$   $\mu\text{m}$  flux measured with VISIR is in good agreement with the Spitzer data, which were taken approximately six months before the MIDI observations. The MIDI spectrum is also consistent with the Spitzer/IRS spectrum longward of  $\sim 10$   $\mu\text{m}$ . However, the Spitzer/IRS spectrum shows a bump at  $\sim 8$   $\mu\text{m}$ , which is not seen in the MIDI spectrum. Evans et al. (2015) reported this feature and the one at  $\sim 6.2$   $\mu\text{m}$  as the unidentified infrared emission, which is commonly attributed to polycyclic aromatic hydrocarbons or PAH (e.g., Allamandola et al. 1999). Evans et al. (2015) show that the Spitzer spectrum taken on 2006 October 24 (MJD54032) also exhibit the PAH features at  $6.2$  and  $8$   $\mu\text{m}$ , which suggests that the PAH emission was stably present over a little more than a year from October 2006 to December 2007. Therefore, it is not very likely – if not entirely excluded – that the PAH emission disappeared entirely

<sup>3</sup> The IRS was a collaborative venture between Cornell University and Ball Aerospace Corporation funded by NASA through the Jet Propulsion Laboratory and Ames Research Center.

<sup>4</sup> Downloaded from <https://sha.ipac.caltech.edu/applications/Spitzer/SHA/>

within six months between the Spitzer observation in December 2007 and our MIDI observations in June 2008. The absence of the PAH emission in the MIDI spectrum can be due to a smaller field of view of 200 mas of MIDI compared to the slit widths of  $3'6-10'7$  of Spitzer/IRS, which suggests that the PAH emission may originate from an extended region. Given that the central star is now H-deficient, the recently rejected inner circumstellar matter should also be H-deficient, from which PAH emission is not expected. Therefore, the PAH emission likely originates from the older, outer circumstellar material ejected before the star became H-deficient. This is consistent with the above observations. However, the UV radiation required to give rise to the PAH emission cannot penetrate the optically thick dust envelope suggested by our modeling presented below. We return to this point in Sect. 4.

#### 4. Modeling of the dust envelope

We carried out radiative transfer modeling with DUSTY (Ivezić et al. 1999) for the observed  $N$ -band visibilities and the spectral energy distribution (SED). The circumstellar envelope of FG Sge is considered to be complex, given the R CrB-like light curve that suggests the formation of clumpy dust clouds or episodic mass loss. However, the present MIDI data are insufficient for constraining such complex structures. Therefore, we assumed spherical shell models to constrain the global properties of the dusty environment of FG Sge.

In the present work, we adopted a distance of  $3.0^{+1.2}_{-1.0}$  kpc derived by Chornay et al. (2021)<sup>5</sup> based on the Gaia Early Data Release 3 (Gaia Collaboration 2021). The bolometric flux of the central star was obtained from the SED obtained before the onset of the mass ejection in 1992. Jurcsik & Montesinos (1999) presented the photometric data from the  $V$  to  $N$  band obtained from June to August in 1983, which they fit with a photospheric model with  $T_{\text{eff}} = 5500$  K and  $\log g = 1.5$ . We obtained a bolometric flux of  $1.72 \times 10^{-11}$  W m<sup>-2</sup> by integrating this SED, which translates into a luminosity of  $4850^{+4600}_{-2690} L_{\odot}$  with the distance of  $3.0^{+1.2}_{-1.0}$  kpc. It should be noted that the large uncertainty in the distance (hence in the luminosity) does not affect the fit to the SED and visibility, because the luminosity of the model star increases as  $\propto d^2$ , but the flux predicted at the distance of the Earth decreases as  $\propto d^{-2}$ , resulting in the same predicted flux. Likewise, the inner radius of the dust shell increases as  $\propto \sqrt{L} \propto d$ , but its angular size remains unaffected because it follows  $\propto d^{-1}$ .

To obtain the SED observed as contemporaneously as possible with our MIDI observations, we used the visible ( $V$ ,  $R$ ,  $I$ , and  $R_c$  bands) photometric data taken on MJD54642 (just three days after our MIDI observations) by Arkhipova et al. (2009) and the infrared ( $JHKLM$ ) photometric data taken on MJD54659.5 (20 days after the MIDI observations) by Shenavrin et al. (2011). As presented above, the MIDI spectrum and VISIR  $19.5 \mu\text{m}$  flux are in agreement with the Spitzer spectrum obtained in December 2007 except for the PAH emission. Therefore, we used these data to cover the mid-infrared region of the SED. We adopted  $E(g-r) = 0.23$  based on the 3D extinction map of Green et al. (2019)<sup>6</sup> for the distance of 3.0 kpc and converted it to  $E(B-V) = 0.202$  using the relations given in Schlafly et al. (2011). This translates into  $A_V = 0.63$  with  $R_V = 3.1$  assumed. The observed SED was dereddened by applying the wavelength

dependence of the interstellar extinction from Cardelli et al. (1989).

The effective temperature of the central star is controversial. Jeffery & Schönberner (2006) concluded that FG Sge had been maintaining  $T_{\text{eff}} \approx 5500$  K since 1980 (as of 1995) and, therefore, proposed that this  $T_{\text{eff}}$  might be the lowest limit in its redward evolution. On the other hand, Fadeyev (2019) derived  $T_{\text{eff}} = 4445$  K based on theoretical modeling of FG Sge's pulsation. We treated  $T_{\text{eff}}$  as a free parameter and calculated models with  $T_{\text{eff}} = 4500, 5000, \text{ and } 5500$  K. Combined with the luminosity of  $4850 L_{\odot}$ , these values of  $T_{\text{eff}}$  correspond to a stellar radius of 115, 93, and 77  $R_{\odot}$ , respectively.

Given the C-rich nature of the photosphere and the circumstellar envelope, we assumed amorphous carbon for the dust grains around FG Sge. We adopted a grain size of  $0.01 \mu\text{m}$  as concluded by Arkhipova et al. (2022) to explain the SED before 2019. The density distribution of dust grains was assumed to be  $\propto r^{-p}$ , where  $p$  is a free parameter, and characterized by the dust condensation temperature ( $T_c$ ), which determines the inner radius of the envelope ( $r_{\text{in}}$ ), and the optical depth in the radial direction at  $0.55 \mu\text{m}$  ( $\tau_V$ ). The outer radius ( $r_{\text{out}}$ ) of the circumstellar envelope was estimated in the following manner. Gonzalez et al. (1998) measured an outflow velocity of  $\sim 200$  km s<sup>-1</sup> from the Na I D lines. Because the mass ejection started in August 1992, the material should have traveled  $1.0 \times 10^{16}$  cm (670 AU) at the time of our MIDI observations in June 2008. On the other hand, DUSTY models show that the inner radius of the envelope ranges from 25 to 40  $R_{\star}$  for  $T_{\text{eff}} = 4500$  to 5500 K for a condensation temperature of  $\sim 1000$  K. Using the above values of  $R_{\star}$ , the inner radius is estimated to be  $(1-3) \times 10^{14}$  cm. Therefore, the maximum distance that the ejected material traveled ( $1.0 \times 10^{16}$  cm) corresponds to 33–100  $r_{\text{in}}$ . We adopted a fixed value of 70  $r_{\text{in}}$ .

We computed models with  $T_{\text{eff}} = 4500, 5000, \text{ and } 5500$  K,  $p = 2.0 \dots 4.0$  ( $\Delta p = 0.5$ ),  $T_c = 800 \dots 1600$  K ( $\Delta T_c = 200$  K), and  $\tau_V = 5 \dots 30$  ( $\Delta \tau_V = 5$ ). However, we found no model that can reasonably reproduce the observed SED and  $N$ -band visibilities simultaneously. For example, the models with the density profile  $\propto r^{-2}$ , which corresponds to stationary mass loss with a constant outflow velocity, can fit the observed SED very well, but they systematically predict the  $N$ -band visibility to be much lower ( $\lesssim 0.5$ ) than the observed data, because the dust envelope appears to be much more extended than the observed data suggest. The models with steeper density profiles can explain the observed  $N$ -band visibilities. However, these models predict the flux longward of  $\sim 10 \mu\text{m}$  to be too low compared to the observed data, because there is too little cold material in the outer region of the envelope.

It is possible that the density profile is steeper than the  $r^{-2}$  in the inner region of the dust envelope before the velocity reaches its terminal velocity. We attempted to explain the observed data with models in which the density profile falls as  $r^{-p}$  from the inner radius  $r_{\text{in}}$  to a certain radius  $r_{\text{tr}}$  and then changes to  $r^{-2}$ . Because the above model grid shows that  $\tau_V$  should be below  $\sim 10$  to explain the visible part of the observed SED, we calculated models with the following parameter ranges:  $T_{\text{eff}}$  (K) = 4500, 5000, and 5000;  $\tau_V = 4.0 \dots 10.0$  ( $\Delta \tau_V = 2.0$ );  $T_{\text{in}}$  (K) = 800  $\dots$  1600 ( $\Delta T_{\text{in}} = 100$  K);  $p = 2.5 \dots 4.5$  ( $\Delta p = 0.5$ ); and  $r_{\text{tr}}/r_{\text{in}} = 2.5, 5, 10, 15, \text{ and } 20$ . Figure 3 shows one of the best-fit models, which reproduces the observed SED and  $N$ -band visibilities fairly well. The model is characterized by  $T_{\text{eff}} = 5000$  K,  $\tau_V = 8$ ,  $T_{\text{in}} = 1100$  K ( $r_{\text{in}} = 33 R_{\star}$ ),  $p = 3.5$ , and  $r_{\text{tr}} = 5 r_{\text{in}}$ . The model still predicts the flux to be somewhat lower than the observed data longward of  $20 \mu\text{m}$ , and the model visibilities are

<sup>5</sup> The errors in the distance correspond to the 84th and 16th percentile of the distance posterior.

<sup>6</sup> <http://argonaut.skymaps.info>

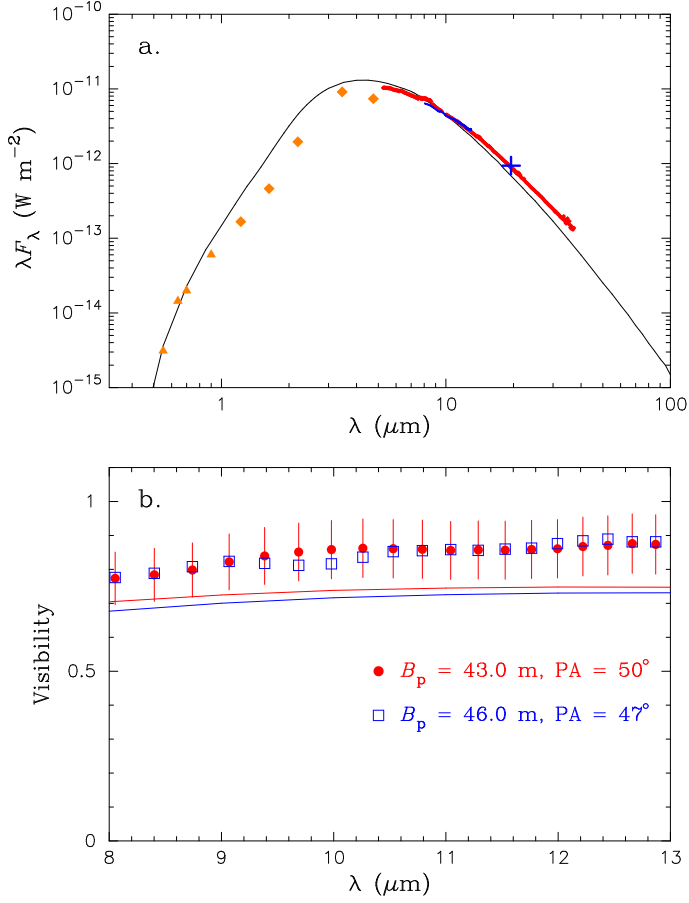


**Fig. 3.** Comparison of a spherical shell model with the observed SED and  $N$ -band visibilities of FG Sge. The model is characterized with  $T_{\text{in}} = 1100$  K, a piecewise power-law density profile with  $r^{-3.5}$  ( $r_{\text{in}} \leq r \leq r_{\text{tr}}$  with  $r_{\text{in}} = 33 R_\star$  and  $r_{\text{tr}} = 5 r_{\text{in}}$ ) and  $r^{-2}$  ( $r > r_{\text{tr}}$ ),  $\tau_V = 8$ , and  $T_{\text{eff}} = 5000$  K. **a:** Observed SED. Orange filled triangles correspond to visible photometric data from Arkhipova et al. (2009). Orange filled diamonds are the infrared photometric data from Shenavrin et al. (2011). The photometric data were dereddened with  $A_V = 0.63$ . The thick solid red line is the Spitzer/IRS spectrum. The thin solid blue line corresponds to the MIDI spectrum. The blue cross corresponds to VISIR photometry. The DUSTY model is shown with the solid black line. **b:** Observed visibilities are shown in the same manner as in Fig. 1a. The solid red and blue lines represent the model visibilities predicted for the 43.0 and 46.0 m baselines, respectively.

slightly lower than the MIDI data. Decreasing  $p$  and/or  $r_{\text{tr}}$  makes the fit to the SED better, but such models predict the  $N$ -band visibilities to be even lower, because their density profiles become similar to  $r^{-2}$ . Our model grid constrains the parameter ranges as follows:  $\tau_V = 8 \pm 2$ ,  $T_{\text{in}} = 1100 \pm 100$  K,  $p = 3.5 \pm 0.5$ , and  $r_{\text{tr}} = 10 \pm 5$ . We cannot constrain  $T_{\text{eff}}$  of the central star within the adopted range between 4500 and 5500 K, because it is heavily obscured.

Recently, Arkhipova et al. (2022) modeled the SED observed from 0.4 to 5.0  $\mu$ m in 2019 with a density profile of  $\propto r^{-2}$  and obtained an optical depth of 4.5 at 0.55  $\mu$ m, which is significantly lower than the  $8 \pm 2$  derived in the present work. This is because they modeled the photometric data taken in 2019, when the dust clouds temporarily cleared. The central star became visible with  $V \approx 13$ , which is  $\sim 4$  magnitude fainter than the  $V \approx 9$  before

the start of the dust formation in 1992. With  $\tau_V = 0.921 \times \Delta V$  (if scattered light and dust thermal emission are ignored),  $\tau_V$  is estimated to be 3.7, which is in broad agreement with 4.5 as derived from their modeling. As mentioned above, the models with the density profile  $r^{-2}$  can explain the observed SED, but not the  $N$ -band visibilities. Given that Arkhipova et al. (2022) only modeled the SED taken at a different epoch (May 2019) from ours, we cannot draw the conclusion that the difference in the density profile reflects the lack of spatially resolved data in the modeling or a temporal variation in the density profile.

The remaining discrepancy between the best-fit models and the observed data is likely due to the complex, clumpy nature of the circumstellar environment of FG Sge as inferred from the irregular, R CrB-like declines in the light curve. Furthermore, a disk-like or ring-like structure may also be present, as observed in the other two born-again objects’ Sakurai’s object and V605 Aql (Chesneau et al. 2009; Hinkle et al. 2014, 2020; Clayton et al. 2013). As described in Sect. 2, if the PAH emission indeed originates from the outer region of the circumstellar envelope, the UV radiation should escape the optically thick envelope. The clumpy and/or disk-like structures can provide a natural explanation for the UV radiation to escape and excite the carrier of the PAH emission even if it is located farther away from the star.

## 5. Discussion and concluding remarks

The dust mass obtained from the model shown in Fig. 3 is  $7.4 \times 10^{-7} M_\odot$ , adopting a bulk density of 2.25 g cm<sup>-3</sup> for amorphous carbon (Gilman 1974). If we assume a gas-to-dust ratio of 200, the total envelope mass is  $1.5 \times 10^{-4} M_\odot$ . Given that the mass ejection started in 1992, the average mass-loss rate at the time of the MIDI observations in 2008 is  $9.3 \times 10^{-6} M_\odot \text{ yr}^{-1}$ . The dust mass of FG Sge seems to be lower than  $6 \times 10^{-5} M_\odot$  as found in Sakurai’s object (Chesneau et al. 2009) and  $\sim 2 \times 10^{-3} M_\odot$  as derived for V605 Aql (Clayton et al. 2013). The difference in the ejected mass may be related to the difference in the nature between FG Sge and the other two final-flash objects – Sakurai’s object and V605 Aql are VLTP objects, while FG Sge is likely to be an LTP object. However, follow-up observations of FG Sge would be necessary to study the long-term variation of the mass of the ejected dust.

As the light curve published by Arkhipova et al. (2022) shows, FG Sge is still experiencing the continuous ejection of dusty material. If we adopt the outflow velocity of 200 km s<sup>-1</sup> as inferred from the Na I D lines, the material at the outer radius of the dust envelope in 2008 should have traveled 560 au ( $\sim 1200 R_\star$ ) by now, which translates into an angular displacement of 190 mas at the distance of 3.0 kpc. While the farthest (thus the coldest) material at the outer boundary may not be detectable in the 10  $\mu$ m region, temporal variations in the circumstellar envelope can be expected. Furthermore, given the presence of disk-like structures in Sakurai’s object and V605 Aql, it is of great interest to study whether FG Sge has a disk or bipolar structures. To better constrain the structure and evolution of the circumstellar environment of FG Sge, interferometric measurements at more baselines and at multiple epochs are indispensable, which can be carried out with the VLTI/MATISSE instrument (Lopez et al. 2022).

*Acknowledgements.* We thank the VLTI team at ESO and the MIDI team for carrying out the observations and making the data reduction software publicly available. K.O. acknowledges the support of the Agencia Nacional de Investigación Científica y Desarrollo (ANID) through the FONDECYT Regular

grant 1210652. This research made use of the SIMBAD database, operated at the CDS, Strasbourg, France.

## References

- Allamandola, L. J., Hudgins, D. M., Sandford, S. A. 1999, *ApJ*, 511, L115
- Arenou, F., Grenon, M., & Gómez, A. 1992, *A&A*, 258, 104
- Arkhipova, V. P., Esipov, V. F., Ikonnikova, N. P., Komissarova, G. V., & Shugarov, S. Yu. 2009, *Astronomy Letters*, 35, 534
- Arkhipova, V. P., Ikonnikova, N. P., Shenavrin, V. I., et al. 2022, *Astronomy Letters*, in press, <https://arxiv.org/abs/2206.02493>
- Blöcker, T. 2001, *Ap&SS*, 275, 1
- Bourges, L., Mella, G., Lafrasse, S., et al. 2017, *JMMC Stellar Diameters Catalogue Version 2*
- Cardelli, J. A., Clayton, G. C., & Mathis, J. S. 1989, *ApJ*, 345, 245
- Chesneau, O., Meilland, A., Rivinius, T., et al. 2005, *A&A*, 435, 275
- Chesneau, O., Clayton, G. C., Lykou, F., et al. 2009, *A&A*, 493, L17
- Clayton, G. C. 1996, *PASP*, 108, 225
- Clayton, G. C., Kerber, F., Pirzkal, N., et al. 2006, *ApJ*, 646, L69
- Clayton, G. C., Bond, H. E., Long, L. A., et al. 2013, *ApJ*, 771, 130
- Chornay, N., & Walton, N. A. 2021, *A&A*, 656, A110
- Evans, A., Gehrz, R. D., Helton, L. A., & Woodward, C. E. 2015, *EAS Publications Series*, Vol. 71–72, 281
- Evans, A., Gehrz, R. D., Woodward, C. E., et al. 2020, *MNRAS*, 493, 1277
- Fadeyev, Yu. A. 2019, *Astronomy Letters*, 45, 655
- Gaia Collaboration (Brown, A. G. A., et al.) 2021, *A&A*, 649, A1
- Gehrz, R. D., Woodward, C. E., Temim, T., Lyke, J. E., Mason, C. G. 2005, *ApJ*, 623, 1105
- Gilman, R. C. 1974, *ApJS*, 28, 397
- Gonzalez, G., Lambert, D. L., Wallerstein, G., et al. 1998, *ApJS*, 114, 133
- Green, G. M., Schlafly, E., Zucker, G., Speagle, J. S., & Finkbeiner, D. 2019, *ApJ*, 887, 93
- Herwig, F. 2005, *ARA&A*, 43, 435
- Herwig, F., Blöcker, T., Langer, N., & Driebe, T. 1999, *A&A*, 349, L5
- Hinkle, K. H., & Joyce, R. R. 2014, *ApJ*, 785, 146
- Hinkle, K. H., Joyce, R. R., Matheson, T., Lacy, J. H., & Richter, M. J. 2020, *ApJ*, 904, 34
- Houck, J., Roellig, T., van Cleve, J., et al. 2004, *ApJS*, 154, 18
- Iben, I., Jr. 1976, *ApJ*, 208, 165
- Iijima, T., & Strafella, F. 1993, *Inf. Bull. Variable Stars*, 3959, 1
- Ivezić, Ž., Nenkova, M., Elitzur, M. 1999, *User Manual for DUSTY*, University of Kentucky Internal Report, accessible at <http://www.pa.uky.edu/moshe/dusty>
- Jaffe, W. 2004, *SPIE Proc.*, 5491, 715
- Jeffery, C. S., & Schönberner, D. 2006, *A&A*, 459, 885
- Jurcsik, J., & Montesinos, B. 1999, *New Astronomy Reviews*, 43, 415
- Kipper, T., & Kipper, M. 1993, *A&A*, 276, 389
- Lagage, P. O., Pel, J. W., Authier, M., et al. 2004, *The Messenger*, 117, 12
- Langer, G. E., Kraft, R. P., & Anderson, K. S. 1974, *ApJ*, 189, 509
- Lawlor, T. M., & MacDonald, J. 2003, *ApJ*, 583, 913
- Leinert, Ch., Graser, U., Przygodda, F. 2003, *Ap&SS* 286, 73
- Leinert, Ch., van Boekel, R., Waters, L. B. F. M., et al. 2004, *A&A*, 423, 537
- Lopez, B., Lagarde, S., Petrov, R. G., et al. 2022, *A&A*, 659, A192
- Miller Bertolami, M. M., Althaus, L. G., Serenelli, A. M., & Panei, J. A. 2006, *A&A*, 449, 313
- Ohnaka, K., Driebe, T., Weigelt, G., & Wittkowski, M. 2007, *A&A*, 466, 1099
- Ohnaka, K., Driebe, T., Hofmann, K.-H., Weigelt, G., & Wittkowski, M. 2008, *A&A*, 484, 371
- Przygodda, F., Chesneau, O., Graser, U., Leinert, Ch., & Morel, S. 2003, *Ap&SS*, 286, 85
- Reindl, N., Rauch, T., Miller Bertolami, M. M., Todt, H., & Werner, K. 2017, *MNRAS*, 464, L51
- Schlafly, E. F., & Finkbeiner, D. P. 2011, *ApJ*, 737, 103
- Schönberner, D. 2008, *ASP Conf. Ser.* 391, 139
- Shenavrin, V. I., Taranova, O. G., & Nadzhip, A. E. 2011, *Astronomy Reports*, 55, 31
- van Hoof, P. A. M., Hajduk, M., Zijlstra, A. A., et al. 2007, *A&A*, 471, L9
- Werner, M. W., Roellig, T. L., Low, F. J., et al. 2004, *ApJS*, 154, 1
- Zhao-Geisler, R., Quirrenbach, A., Köhler, R., Lopez, B., & Leinert, C. 2011, *A&A*, 530, A120